FULL RESEARCH ARTICLE

A mechanical model in wire + Arc additive manufacturing process

E. A. Bonifaz[1] · J. S. Palomeque[1]

Abstract

Material properties are dependent upon the microstructural characteristics of the part. Developing an accurate and sufficient representation of the microstructure obtained in metal additive manufacturing (AM) is critical to precisely estimate material properties. Since the material properties for AM parts are an important function of the welding processing parameters, a fundamental understanding of how AM components behave in load-bearing applications depends on understanding the evolution of thermal cycles and residual stresses during component fabrication. In this work, a finite-element thermo-plasticity procedure in wire + arc AM process was developed in a three-dimensional domain using the finite-element (FE) code ABAQUS. The proposed research aims to establish a methodology for characterizing directed energy deposited metals by linking processing variables to the resulting plastic strains and residual stresses. The effect of multi-layer deposition on the prediction and validation of local plastic strains and thermally induced stresses was investigated. It was found that the thermal (residual) stresses increase with either the increase of weld speed or the increase of the heat distribution parameter. On the other hand, local plastic strains increase with the increase of welding speed, but not necessarily with the increase of the heat distribution parameter. Similarly, the level of thermal stresses and local plastic strains is lower in each new successive AM layer. As a new layer is deposited over a previously heated one, the relief of thermal stresses and plastic strains occurs by preheating; the more preheated the previous layer, the less the level of thermal stresses and plastic strains in the successive deposited layer. Furthermore, the lowest level of stresses and strains observed in the last deposited AM layer, it can be solely caused by the hotter previous layer, even though the top unrestrained weldment surface is free to expand. Numerically predicted thermal stresses at different welding layers are presented for further experimental comparison. A firm foundation for thermo-mechanical modelling in wire + arc additive manufacturing process is established.

Keywords Multi-layer deposition · Thermal cycles · Thermal stresses · Plastic strains · The layer build-up process

1 Introduction

Wire + arc additive manufacturing (WAAM) is a layer-by-layer build-up procedure that can be categorized as a form of multipass arc-welding for additive manufacturing (AM) purposes [1]. In multipass welding, multiple welds interact in a complex thermo-mechanical manner. In the AM welding procedure, the current metal layers are deposited on top of previously solidified weld beads. Residual stresses and distortion affect components made by the WAAM process. If not diminished and controlled, these issues threaten the adoption of AM in industry. It must be pointed out that residual stresses are typically measured and validated experimentally using both the contour and the neutron diffraction method. However, the error associated with these techniques creates conflicting opinions in the scientific community. Research to eliminate distortion and residual stresses using high-pressure interpass rolling in wire + arc additive manufacturing components is being conducted in current investigations [2]. Nonetheless, the interaction of residual stresses with localized stress concentrations and crack-like defects must also be taken into account to predict component reliability in load-bearing and thermo-mechanical applications. Compared with other AM processes, the robotic arc-weld additive manufacturing process allows for the fabrication of complex geometries, uses cheaper filler materials, has a

✉ E. A. Bonifaz
ebonifaz@usfq.edu.ec

J. S. Palomeque
juansepa@live.com.ar

1 Mechanical Engineering Department, Universidad San Francisco de Quito, Diego de Robles entre Francisco de Orellana y Pampite, 170901 Cumbayá, Ecuador

higher deposition rate, and requires a lower investment [3]. A component manufactured by the AM "welding" procedure can achieve equivalent mechanical properties to a forged or cast complex component [4]. However, the surface finish and accuracy are questionable. To produce a high-quality part or product, it is important to establish a methodology for characterizing direct energy deposited metals by linking processing variables to the resulting microstructure and subsequent material properties.

Current study on residual stress in AM is in the initial stage, so measurement and simulation methods for macro- and micro-residual stresses, in-process and post-process mitigation, and the impacts on part dimensional accuracy and functionality such as fatigue, creep, and corrosion, remain to be explored [5]. Models required to span the scope of AM processes towards predicting material properties and residual stresses of the final build are discussed in Ref. [6]. It is mentioned that models have to deal with multiple physical aspects such as heat transfer and phase changes as well as the evolution of residual stresses throughout the build time. The modeling task is, therefore, a multi-scale, multi-physics endeavor calling for a complex interaction of multiple algorithms [6]. Few modeling studies have been conducted due to the complexity of the physical process and the scarcity of relevant temperature-dependent material properties. Reliable simulations and experimental measurements of thermal stresses remain to be addressed [7]. The stress–strain evolution in weldments can be predicted using thermal cycles obtained from previous thermal simulations [8–13]. However, the mechanical analysis takes more computer time than the transient temperature analysis [9]. Non-equilibrium phases encountered in the different weld zones appear to be due to the extreme cooling events that follow welding (i.e., different cooling rates). Therefore, the prediction of final microstructures and corresponding mechanical properties in weldments remains a great challenge.

High tensile residual stress formation in the surface zone for metal AM is mainly caused by high-temperature gradient and rapid cooling, while the presence of substrate has a significant influence on residual stress and plastic strain magnitudes [5]. The performance of additively manufactured compositionally graded joints depends on the residual stresses and distortion governed by the cooling process and local mechanical properties of the joint [14]. The difference in the thermo-physical properties between the two end alloys governs the cooling process and thus the evolution of the residual stresses and distortion. Mukherjee et.al. [14], developed a thermo-mechanical model to provide a way to additively manufacture sound-graded joints for minimizing abrupt changes in residual stresses and distortion of dissimilar joints. In that research, it was found that the sharp changes in residual stresses in dissimilar joints can be minimized by fabricating a graded joint between them.

In a previous work [13] designed to find accurate transient temperature distribution in wire + arc additive manufacturing process, a 3D transient non-linear finite-element model to simulate multi-layer deposition of cast IN-738LC alloy onto SAE-AISI 1524 Carbon Steel Substrates was developed. Forced convection and temperature-dependent material properties were included in the model. A moving heat source was applied over the top surface of the plate and on top of previously solidified weld beads. The effect of multi-layer deposition on the prediction and validation of melting pool shape and thermal cycles was also investigated. The effect of convection and radiation heat loss from the layered surfaces was included in the finite-element analysis. As the AM layers act as extended surfaces (fins), it was found that the heat extraction is quite significant. It should be highlighted that the thermal model is good enough to predict accurate time–temperature history and weld profiles. The transient non-linear nature of multiple welds that interact in a complex thermo-mechanical manner increases the computational requirements. Also, the seam volume depends on the number of layers which mainly depend on the wire feed, wire diameter, and welding speed.

As certainty in the WAAM thermal model (based on the element-birth technique) was attained, the purpose of this study was to perform the mechanical counterpart using simulated temperatures as initial conditions. The coupled thermo-mechanical modeling approach typically used in single-pass welding was also used to predict the stress and strain evolution in the WAAM process. The analysis framework is described in a previous work [7]. It is important to point out that microstructure evolution models currently exist only for one melting and solidification step, such as would be encountered during an idealized (e.g., single pass) AM process. These models do not address the formation of non-equilibrium phases or the effect of multiple heating and cooling cycles, such as those encountered in production AM processes. However, in our previous research [13], the mentioned effect and the heat loss (convection and radiation) between the weldment (layers) surfaces and the surroundings were included into the FE analysis. Since the present thermo-mechanical model accurately predicts the evolution of residual stresses and plastic strains resulting from a welding process, a numerical tool to handle the right combination of feedstock material composition and printing parameters is being developed. The numerical tool uses only the composition of the base material, filler material, and welding parameters as input data.

2 The model

The general procedure used to solve the thermo-plasticity problem [7, 15–17] was used in the present work. The von Mises yield criterion is considered here. To prevent rigid-body
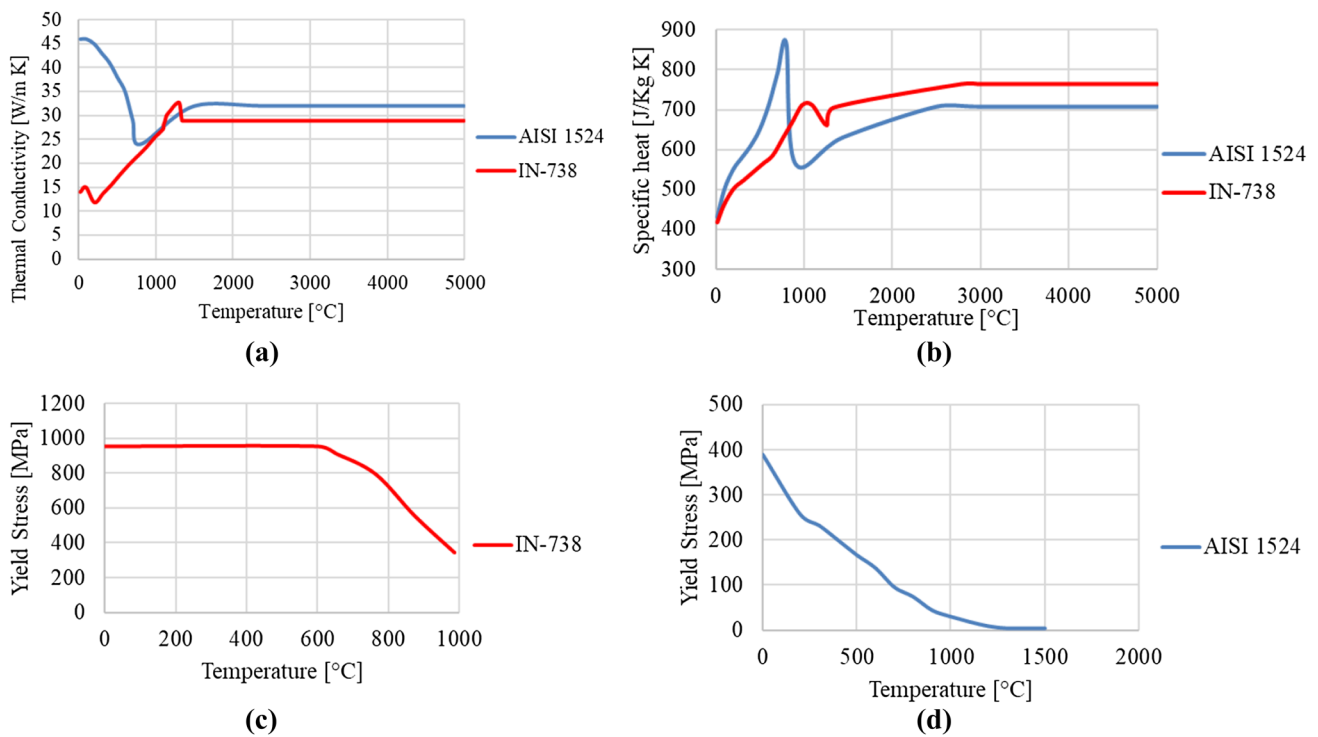
Fig. 1 Physical and mechanical temperature-dependent properties for IN-738 LC alloy and SAE-AISI 1524 steel. **a** Thermal conductivity, **b** specific heat, **c** yield stress of IN-738 LC alloy, and **d** yield stress of SAE-AISI 1524 steel

Table 1 Chemical compositions (%) of alloy IN-738 LC and SAE-AISI 1524 low carbon steel

	Ni	Al	Co	Cr	Mn	Mo	Nb	Si	Ta	Ti	W	C	S	P
Alloy IN-738 LC	61.7	3.52	8.5	15.75	0.01	1.88	0.84	0.04	1.61	3.42	2.51	0.11		
SAE-AISI 1524 steel				1.6				0.5				0.2	0.035	0.03

motion of the entire specimen, essential boundary conditions at each boundary nodal point were specified [18]. The built in type boundary condition ENCASTRE [19] constrained on all displacements and rotations at a node; it was used to represent the fixation of the specimen to the base plate. Temperature-dependent properties documented in Refs. [7, 13, 17, 20] are shown in Fig. 1.

The chemical compositions of the materials used in the present work are presented in Table 1.

Other properties used in the present study are summarized in Table 2.

The welding conditions documented in Table 3 were chosen to solve the 3-D transient non-linear heat conduction (Eq. 1) and equilibrium (Eq. 2) governing differential equations:

$$\frac{\partial}{\partial x}\left(k\frac{\partial T}{\partial x}\right) + \frac{\partial}{\partial y}\left(k\frac{\partial T}{\partial y}\right) + \frac{\partial}{\partial z}\left(k\frac{\partial T}{\partial z}\right) + \dot{Q} = \rho c_p \frac{\partial T}{\partial t}. \quad (1)$$

Table 2 Properties for Alloy IN-738 and SAE-AISI 1524 used in all simulations

Properties	Alloy IN-738	SAE-AISI 1524
Mean coefficient of thermal expansion	13.3×10^{-6} K^{-1}	11.9×10^{-6} K^{-1}
Modulus of elasticity	204 GPa	200 GPa
Density	8.11 g/cm^3	7.82 g/cm^3
Poisson's ratio	0.3	0.3
Surface emissivity	0.7	0.7

Here, ρ is the density, c_p is the specific heat, k is the thermal conductivity, T is temperature, t is time, and $\dot{Q}$ the internal heat source term. In the present research, $\dot{Q}$ is zero and the latent heat was not considered:

Table 3 Welding conditions used for WAAM steel–nickel-based super alloy samples

	Set 1			Set 2		
	Weld 1	Weld 2	Weld 3	Weld 4	Weld 5	Weld 6
Current (amp)	200	200	200	208	208	208
Voltage (V)	14.84	20.78	26.72	21.03	29.45	37.86
Travel velocity (m/min)	0.25	0.35	0.45	0.25	0.35	0.45
Heat input (kJ/m)	712.5	712.5	712.5	1050	1050	1050
Heat distribution parameter C (mm)	3.65			5.3		
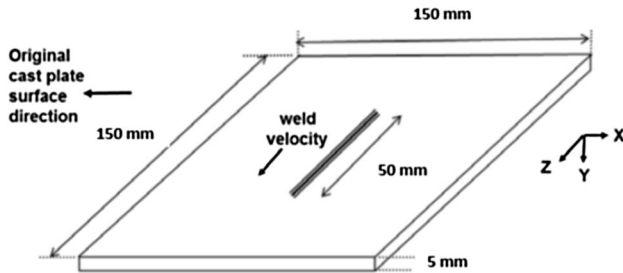
Fig. 2 Schematic of the experimental set-up for AM weld tests

$$\frac{\partial \sigma_{ji}}{\partial x_j} = 0. \tag{2}$$

Here, σ_{ji} is the stress tensor. Details of the thermo-mechanical analysis can be found in the previous works [6, 11, 14, 17].

Figure 2 shows the experimental set-up for AM weld tests considered in the simulations. To observe the heat transference among layers, all welding layers had gluing contacts. The base plate was also modelled and convection (natural and forced) heat-transfer coefficients were implemented into the ABAQUS subroutine FILM. Based on this, the
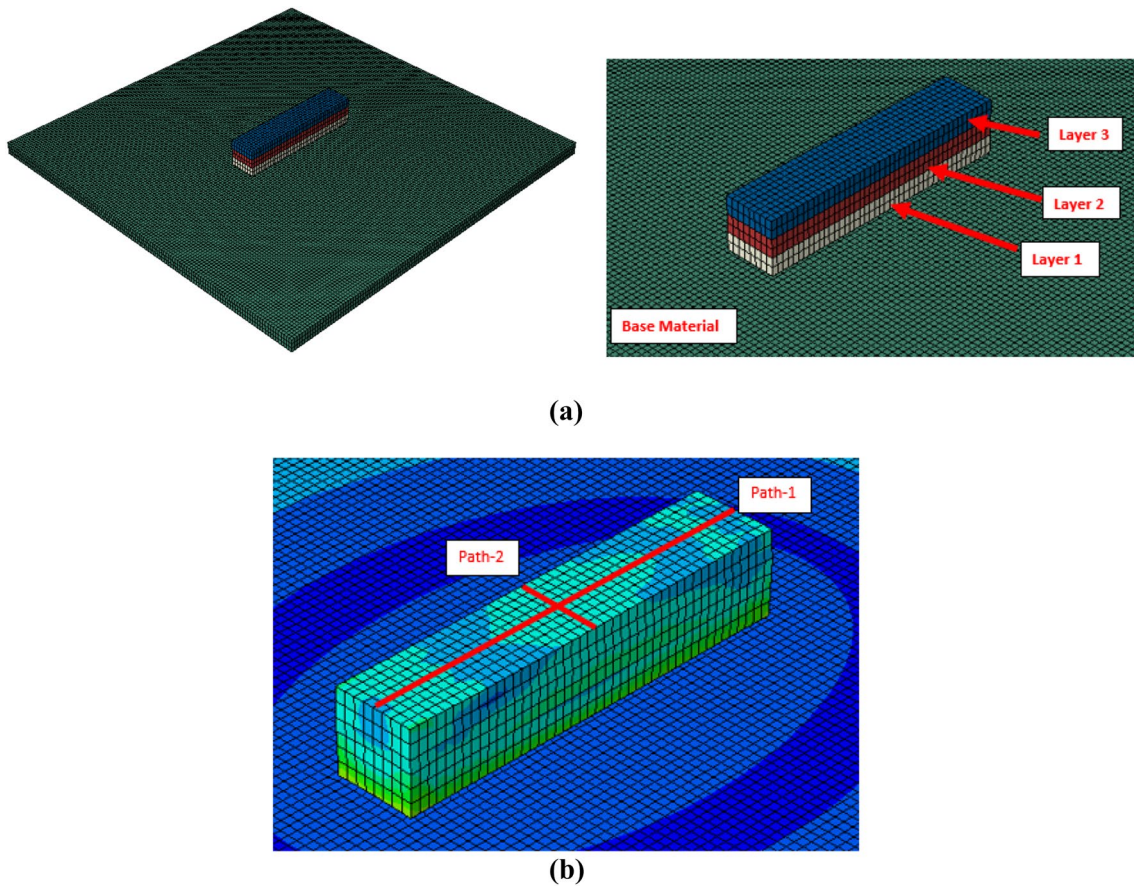

(a)

(b)

Fig. 3 Multiple arc passes meshing scheme created with the ABAQUS * MODEL CHANGE option. **a** Base material and analyzed layers. **b** Selected paths located on Layer 3. Length of path 1 = 50 mm, length of Path 2 = 10.3 mm for welds of set 1, and length of Path 2 = 13.4 mm for welds of set 2. Element type = C3D8

temperature profile in the semi-finished products (layers) was accurately simulated.

3 Results and discussion

Two sets of three welds each are grouped based on the common heat distribution parameter C (see Table 3). The heat distribution parameter C is used to represent the shape and power density distribution of the arc. As the diameter of the arc increases, the power density distribution decreases. Figure 4 shows calculated thermal (Mises) stresses values for the two analyzed sets (Set 1: Welds 1, 2, and 3; and Set 2: Welds 4, 5, and 6) at time step 120 s vs. distance along the path located on Layer 3 (see Fig. 3). Figure 4a shows the Mises stresses calculated through the longitudinal Path 1 of length 50 mm, and Fig. 4b shows the Mises stresses calculated through the transversal Path 2, whose length depends on the heat distribution parameter C. This parameter has influence on Path 2, because as the diameter of the arc increases, the length of Path 2 increases (and vice versa). It can be clearly seen that the thermal (Mises) stresses increase either with the increase of weld speed v, or with the increase of the heat distribution parameter C. Note that the heat input was kept constant in each of the two
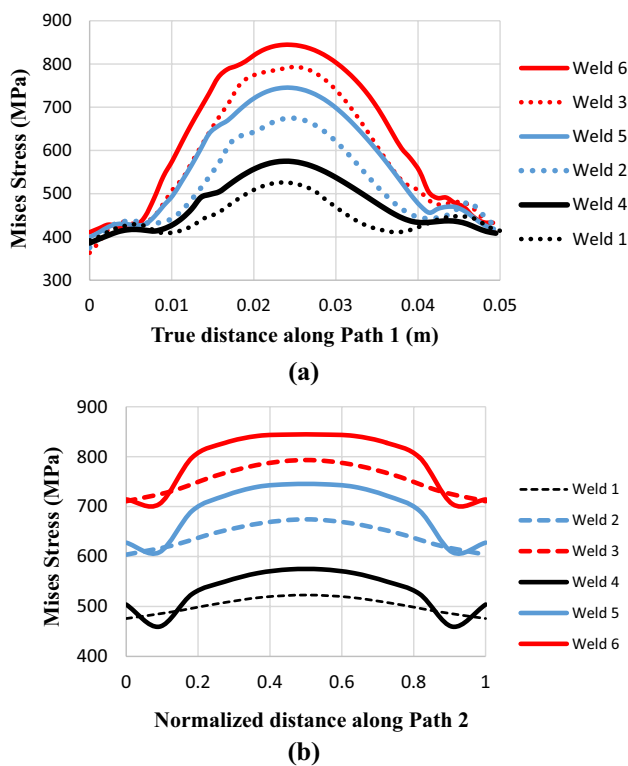
weld sets. It is also observed a concave variation in Mises stresses at the extremes of the transversal path in welds for set 2 ($C = 5.3$ mm). It can be caused by the higher power, bigger C, and the effect of convection and radiation heat loss from the weldment (layers) surfaces that act as extended surfaces (fins).

Figure 5 shows a high level of plastic strains calculated along the paths documented in Fig. 3b. For all the simulations, the highest plastic strains are located near the end of the longitudinal path (see Fig. 5a). This reveals that the presence of substrate has a significant influence on plastic strain magnitudes. Cold base material acts as the restrain source allowing plastic strains to arise in locations around the end of the path. Therefore, PEEQ is highest near the end of the longitudinal Path 1, because plastic strains were partially alleviated. On the other hand, PEEQ decreases from fusion line to centerline (i.e., low in the middle along Path 2), because residual stresses increase from fusion line to centerline (see Fig. 5b). The highest residual stresses appear in regions of highest elastic strains that remain after all external thermal loads were removed in agreement with conventional phenomenological material models, where the macroscopic residual stress is always directly related to the macroscopic elastic strain. Plastic strains also increase with the increase
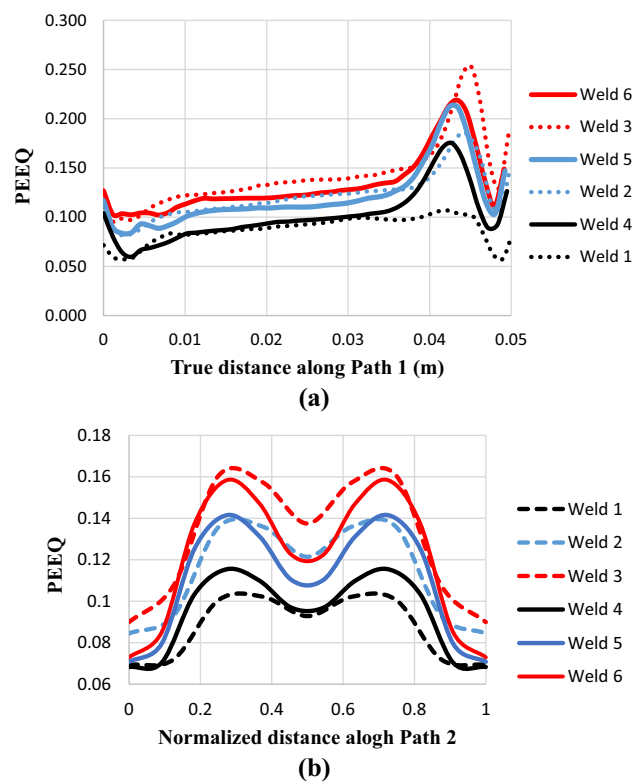

Fig. 4 Mises stresses calculated along path: (a) in the longitudinal Path 1; (b) in the transversal Path 2. Welding conditions documented in Table 3

Fig. 5 Equivalent plastic strains (PEEQ) calculated along path. **a** In the longitudinal Path 1. **b** In the transversal Path 2. Welding conditions documented in Table 3
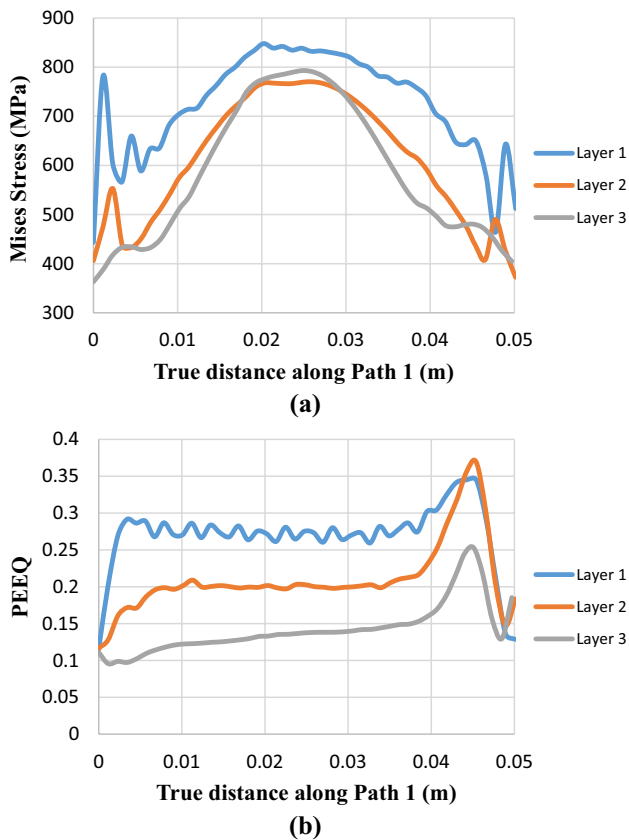
Fig. 6 Mises stresses and equivalent plastic strains (PEEQ) calculated along Path 1 in three different layers of Weld 3 at time step 120 s **a** Mises stresses; **b** equivalent plastic strains (PEEQ). Welding conditions documented in Table 3

Fig. 7 Mises stresses and equivalent plastic strains (PEEQ) calculated along Path 1 in three different layers of Weld 6 at time step 120 s **a** Mises stresses; **b** equivalent plastic strains (PEEQ). Welding conditions documented in Table 3

of welding speed, but not necessarily with the increase of the heat distribution parameter as seen in Fig. 5a, b.

Figure 6 shows Mises stresses and equivalent plastic strains (PEEQ) values calculated along Path 1 in three different layers of Weld 3 at time step 120 s. Figure 7 shows Mises stresses and equivalent plastic strains (PEEQ) values calculated along Path 1 in three different layers of Weld 6 at time step 120 s.

It is observed in Figs. 6 and 7 that the level of Mises stresses and equivalent plastic strains is lower in each new successive AM layer. The order of deposition (Layer 1 → Layer 2 → Layer 3) is shown in Fig. 3a. As a new layer is deposited over a previous heated one, the relief of thermal stresses and plastic strains occurs by preheating (the more preheated the previous layer, the less the level of thermal stresses and plastic strains in the successive deposited layer). Furthermore, the lowest level of stresses and strains observed in the last deposited AM Layer 3 (Figs. 6, 7), it can be solely caused by the hotter previous layer, even though the top unrestrained weldment surface is free to expand.
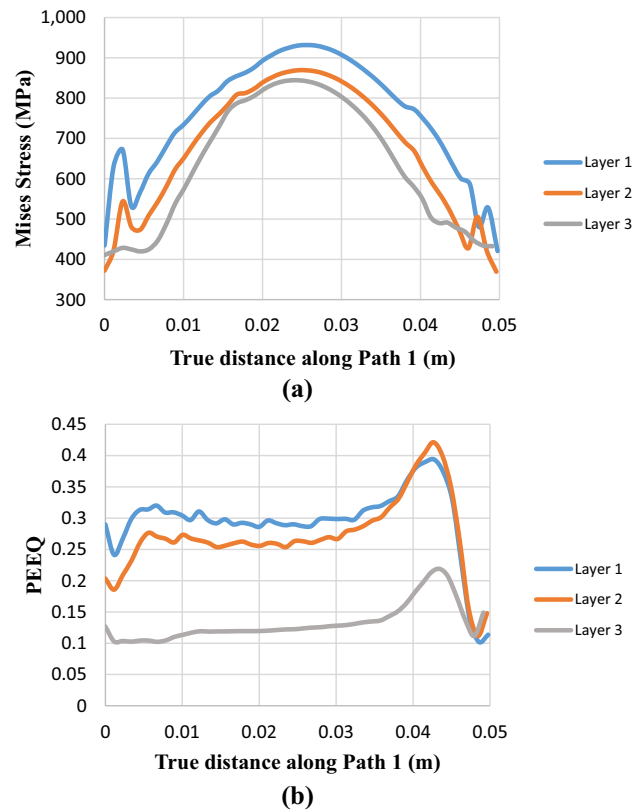
4 Concluding remarks

1. It was found that the thermal (residual) stresses increase with either the increase of weld speed or the increase of the heat distribution parameter. On the other hand, local plastic strains increase with the increase of welding speed, but not necessarily with the increase of the heat distribution parameter.

2. Similarly, the level of thermal stresses and local plastic strains is lower in each new successive AM layer. As a new layer is deposited over a previously heated one, the relief of thermal stresses and plastic strains occurs by preheating; the more preheated the previous layer, the less the level of thermal stresses and plastic strains in the successive deposited layer. Furthermore, the lowest level of stresses and strains observed in the last deposited AM layer, it can be solely caused by the hotter previous layer, even though the top unrestrained weldment surface is free to expand.

3. A firm foundation for thermo-mechanical modelling in wire + arc additive manufacturing process was established.

References

1. Williams SW, Martina F, Addison AC, Ding J, Pardal G, Colegrove P (2016) Wire + arc additive manufacturing. Mater Sci Technol 32(7):641–647
2. Martina F, Roy MJ, Szost BA, Terzi S, Colegrove PA, Williams SW, Withers PJ, Meyer J, Hofmann M (2016) Residual stress of as-deposited and rolled wire + arc additive manufacturing Ti–6Al–4V components. Mater Sci Technol 32(14):1439–1448
3. Graf M, Hälsig A, Höfer K, Awiszus B, Mayr P (2018) Thermo-mechanical modelling of wire-arc additive manufacturing (WAAM) of semi-finished products. Metals 8(12):1009
4. Brandl E, Baufeld B, Leyens C, Gault R (2010) Additive manufactured Ti-6Al-4V using welding wire—comparison of laser and arc beam deposition and evaluation with respect to aerospace material specifications. Phys Procedia 5:595–606
5. Li C, Liu ZY, Fang XY, Guo YB (2018) Residual stress in metal additive manufacturing. In: 4th CIRP Conference on Surface Integrity (CSI 2018). Procedia CIRP, vol 71, pp 348–353
6. Megahed M, Mindt HW, N'Dri N (2016) Metal additive-manufacturing process and residual stress modeling. Integr Mater Manuf Innov 5:61
7. Bonifaz EA (2018) Thermo-mechanical analysis in SAE-AISI 1524 carbon steel gas tungsten arc welds. Int J Comput Mater Sci Surf Eng 7(3/4):269–287
8. Szost BA, Terzi S, Martina F, Boisselier D, Prytuliak A, Pirling T, Hofmann M, Jarvis DJ (2016) A comparative study of additive manufacturing techniques: residual stress and microstructural analysis of CLAD and WAAM printed Ti-6Al-4V components. Mater Des 89:559–567
9. Debroy T, David SA (1995) Physical processes in fusion welding. Rev Mod Phys 67(1):85–112
10. Brown SB, Song H (1992) Implications of three-dimensional numerical simulations of welding of large structures. Weld J 71(2):55-s–62-s
11. Thiessen RG, Richardson IM (2006) Metall Mater Trans B 37B:655–633
12. Kou S (2003) Welding metallurgy, 2nd edn. Wiley, New York
13. Bonifaz EA (2019) Modelling of thermal transport in wire + arc additive manufacturing process. In: Rodrigues J et al (eds) Computational science—ICCS 2019. ICCS 2019. Lecture Notes in Computer Science, vol 11539. Springer, Cham, pp 647–659
14. Mukherjee T, Zuback JS, Zhang W, DebRoy T (2018) Residual stresses and distortion in additively manufactured compositionally graded and dissimilar joints. Comput Mater Sci 143:325–337
15. Dunne F, Petrinic N (2005) Introduction to computational plasticity. Oxford University Press, Oxford
16. Bonifaz EA, Richards NL (2008) The plastic deformation of non-homogeneous polycrystals. Int J Plasticity 24:289–301
17. Bonifaz EA, Richards NL (2010) Stress–strain evolution in cast in-738 superalloy single fusion welds. Int J Appl Mech 2(4):807–826
18. Burnett DS (1988) Finite element analysis: from concepts to applications. Addison-Wesley Publishing Company, Boston
19. ABAQUS 6.14.2 (2014) Finite Element Software. Simulia ABAQUS® Inc
20. Bonifaz EA, Richards NL (2009) Modeling cast In-738 superalloy gas-tungsten-arc- welds. Acta Mater 57:1785–1794